Research Square

Preprints are preliminary reports that have not undergone peer review.
They should not be considered conclusive, used to inform clinical practice,
or referenced by the media as validated information.

Assessing and mapping wind erosion-prone areas in northeastern Algeria using additive linear model, AHP, FAHP approaches, GIS, and medium resolution multisource remotely sensed data

Ali Mihi (mihialieco@gmail.com)
Universite Larbi Tebessi: Universite de Tebessa
Abdelkrim Benaradj
university of Naama

Research Article

Keywords: Wind erosion, empirical model, AHP, FAHP, WLC, data-scarce

Posted Date: April 21st, 2021

DOI: https://doi.org/10.21203/rs.3.rs-369956/v1

License: This work is licensed under a Creative Commons Attribution 4.0 International License.
Read Full License

Assessing and mapping wind erosion-prone areas in northeastern Algeria using additive linear model, AHP, FAHP approaches, GIS, and medium resolution multisource remotely sensed data

Ali Mihi[1*], Abdelkrim Benaradj[2]

[1]Department of Natural and Life Sciences, Faculty of Exact Sciences and Natural and Life Sciences, Larbi Tebessi University,Tebessa 12002. Algeria.

[2]Department of Natural and Life Sciences, Faculty of Sciences and Technology University Center of Salhi Ahmed , Naama 45000, Algeria.

*:Address correspondence to Ali MIHI, Department of Natural and Life Sciences, Faculty of Exact Sciences and Natural and Life Sciences, Larbi Tebessi University, Tebessa 12002. Algeria. E-mail: mihialieco@gmail.com; ali.mihi@univ-tebessa.dz, Cell: +213698214517.

Running title: **Regional Modelling of wind erosion risk in northeastern Algeria**

Number of words (excluding the abstract and references): **7254**

Number of MS pages: **25**

Number of tables: **5**

Number of figure: **9**

Funding: This study was not funded by any source.

Conflicts of interest: The authors declare no conflict of interest.

Abstract

Wind erosion is one of the most severe environmental problems in arid, semi-arid and dry sub-humid regions of the planet. This dissertation aimed to identify areas sensitive to wind erosion in northeastern Algeria (Wilaya of Tebessa) based on empirical model using analytic hierarchy process (AHP), fuzzy analytic hierarchy process (FAHP) approaches, and geomatics-based techniques. Sixteen causative factors were used incorporating meteorological, soil erodibility, physical environment, and anthropogenic impacts as main available inputs in this approach. Weighted linear combination (WLC) algorithm was used to combine all standardized raster layers. Area under curve (AUC) value equal 0.96 indicate an excellent accuracy for the

proposed approach. Globally, wind erosion risk increase gradually from the north to south of the whole area. Besides, it was found that areas with slight, moderate, high, and very high covered 9.65 %, 25.83 %, 24.30 %., and 40.22 %, respectively of the total. Our results highlighted the potential of additive linear model, and free available medium resolution multi-source remote sensing data in studying natural hazards and disasters mainly under data-scarce or areas of difficult access in developing countries. In addition, restoration and re-vegetation activities of sensitive areas at high risk of wind erosion represent a challenge for researchers and decision-makers.

Keywords: Wind erosion, empirical model, AHP, FAHP, WLC, data-scarce

Introduction

Soil is essentially a non-renewable resource on the human time scales. It is dynamic is prone to rapid degradation depending on land misuse and soil mismanagement (Blanco and Lal, 2008). Among the different erosive processes acting on the surface of the earth, wind erosion or desertification caused by wind erosion and aeolian processes is one of the environmental problems in many parts of the world (Panagos and Katsoyiannis, 2019). Specifically, wind erosion affecting mostly arid, semi-arid and semhumid areas in the world because of limited vegetative cover and harsh climate (Ravi et al., 2011). In fact, wind erosion is a process of wind-forced movement of soil particles by removing soil from one place and depositing it in another (Zheng, 2009). Overall, its occurs when the force of wind exceeds the threshold level of gravity and cohesion of the soil particles at surface (Goudie and Middleton, 2006). Generally, there are three different phases during wind erosion process; (i) initiation of the soil particle movement (detachment or deflation), (ii) soil particle transportation (suspension, saltation and surface creep), and (iii) deposition of soil particles. Collectively, wind erosion is the result of complex interactions of many factors, the most sensitive parameters influencing wind erosion include atmospheric conditions (e.g. wind intensity, precipitation and temperature), soil properties (e.g. soil texture, composition and aggregation), land-surface characteristics (e.g. topography, soil surface water content, roughness, and vegetative cover) and land use/land change practice (e.g. anthropogenic and agricultural activities) (Shao, 2008). As result, wind erosion had significant effects on soil, plant and human life in numerous ways by reducing soil fertility, affecting plant emergence, quality and yield, and increasing air pollution. Furthermore, it is one of the processes leading to desertification (Hong et al., 2020). Here, understanding the spatiotemporal

aeolian processes is extremely important in the process of planning and management of natural resources for both scholars and policymakers.

Recently, wind erosion represent the major cause of the world land degradation in arid and semiarid. On a global scale, wind erosion damaged an estimated 5.05 million/km^2, accounting for 46.4 % of world degraded land **.** At the continental scale, Africa having the maximum size for wind erosion areas with 159.8 M ha. It is followed by Asia with 153.1 M ha, and then Europe, North America, and America with 38.7 Mha, 37.8 Mha, 26.9 Mha, respectively, and finally Australasia with only 15.9Mha. Within Africa continent, the Great Sahara (largest hot desert in the world), occupies ~ 30% of African continent total surface area. It covers ten countries including Algeria. It stretches in length for approximately 5,600 km from the atlantic coast to the shores of the Red Sea. In prior research, dust-source areas in North Africa are not fully consistent in the previous studies. Actually, Algeria and Niger are one of the main four major source areas for the dust in North Africa (Ravi et al., 2011). In Algeria country, dust source is located between chott melrhir (Algeria) and chott Jerid (Tunisia). Consequently, high dust concentration occurs principally at the south of the Algerian saharan atlas region (Shao, 2008). As result, about 20 Mha are threatened by wind erosion in Algeria (Bensaïd, 2006). Covering a total area of 20 million ha, Algerian steppes are the most widely distributed rangeland types in the North African countries (Hirche et al., 2011). In Algeria, change in climatic and soil conditions make the steppe a fragile environment. Unfortunately, about 600 000 ha of Algerian steppes have been degradation by wind erosion (Bensaïd, 2006).

Wind erosion phenomenon is complex process and cannot be directly measured soils losses at a field scale (Webb et al., 2009). To assess wind erosion land susceptibility, there are numerous empirical wind-erosion modelling, change in its complexity, input data required, model outputs elaborated, and their application scales, such as, Wind Erosion Equation (WEQ) (Woodruff and Siddoway, 1965), Wind Erosion Prediction System (WEPS) (Hagen, 1991), Agricultural Policy/Environmental eXtender (APEX) (Williams et al.,1995), Revised Wind Erosion Equation (RWEQ) (Fryrear et al., 1998), Texas Erosion Analysis Model (TEAM) (Gregory et al., 1999), Wind Erosion on European Light Soils (WEELS) (Böhner et al., 2003), Single-event Wind Erosion Evaluation Program (SWEEP) (Tatarko et al., 2019). In recent years, new techniques have been used to evaluate wind erosion vulnerability. For instance, fuzzy logic (Saadoud et al, 2018; Yang et al. 2021), Bayesian Belief Network (BBNs) (Kouchami-Sardoo et al., 2019), Artificial Neural Networks (ANNs) (Huang et al., 2006), Bivariate Statistical models (Ettoumi et al., 2003), Analytic Hierarchy Process (AHP) (Yu et al., 2011), and

Fuzzy *C*-Means Clustering (FCM) (Shi et al., 2010). Indeed, AHP and hybrid Fuzzy Analytic Hierarchy Process (FAHP) are widely used for complex decision making problems and model prediction by both decision makers and scholars due to its nature to make the best optimal decisions possible compared to other Multi Criteria Decision Making (MCDM) methods (Shapiro and Koissi, 2017).

Modelling wind erosion hazard can provide useful tools to researchers of erosion process and factors, land users, technical experts, and policy makers for better understanding of this phenomenon as well as play a crucial role in developing successful strategies and sustainable planning and management in land rehabilitation and wind erosion control projects. Indeed, quantifying the wind soil erosion hazard using the existing models (WEQ/RWEQ, WEPS, APEX…etc.) requires precise data with complex structures on a very fine scale. Besides, the choice of a model should be adapted with limited available inputs data influencing wind erosion phenomenon. Here, availability of these data represent a challenge in developing countries, due to lack of resources and poor infrastructure for continuous monitoring of environmental variables. Furthermore, most of these models are designed to estimate wind erosion risk at a local scale, as well as, it's scaled up into a regional-scale still discutable and not fully consistent. Against this background, the aim of this dissertation is: (i) the quantitative estimate of the wind erosion vulnerability at a regional scale in the whole area of Tebessa (NE Algeria) using WLC algorithm ,AHP, fuzzy AHP (FAHP) approaches, GIS, and remote sensing techniques (ii) to prove the potential of using available medium resolution multi-source remote sensing data for monitoring and assessing natural hazard, (iii) to provides scholars, policy makers, planner, and expert of environment specialist an accurate maps of wind erosion sensitivity, in order to adopt the best strategies in land restoration and wind erosion control programs.

Materials and Methods

Study area

Geographically, the study area (Wilaya of Tebessa) is located at northeastern of Algeria, it stretches within northern latitudes of 35°10′to 35°22′and eastern longitudes of 7°13′ to 7°55′, covering a total area of ~ 13,261 km^2 (Fig.1a). Administratively, it incorporates 28 municipalities. The elevation of the area ranges from – 1 and +1713 above sea level. The study area has a semi-arid Mediterranean climate (Fig. 1b). According the ombrothermic diagrams of Gaussen and Bagnouls, the dry season lasts five months a year (Fig.1c), with hot and dry summers (average annual temperature =15.84 °C) and mild winters with low rain (mean annual rainfall=379.77 mm). The hottest month is July (27.26C°), while the coldest month is January

(6,47C°). The wettest month is September (43.41 mm), while the driest month is July (14.37 mm) (Djellab et al. 2019). Annual wind speeds are weak to moderate (from 0.34 to 10.57 m/s) (Fig. 6f). Seasonally, the high wind speeds values are recorded in spring season. In fact, the most frequent surface winds blow mainly from the North and Northwest (46 %) bringing rain during the wet season, and soften the climate by reducing hot weather during the summer months, although other wind directions are southeast and southwest (32%), this winds called sirocco are hot and dry and blows from the Sahara to the north in summer period (Seltzer, 1946). In fact, the areas represent the mountain morphologies (Aurès Nemamcha Mountains in the north of wilaya) act as barriers in the way of sirocco wind, which make the north of Wilaya not very exposed to this wind type. Additional to the livestock farming of sheep, agriculture is the main human activity with ~ 27.7% of the whole area (irrigated and rainfed crop cultivation). The naturel vegetation is dominated by steppe type with 30%. Six main soil types are distinguished in the study area—calcic, calcareous, basic alluvial, saline soil, and aeolian soil of ablation. The lithological formations can be subdivided into four groups according to their friability—very resistant materials (limestone and dolomite); resistant materials (Friable limestone); vulnerable materials (marls, conglomerates, and sandstone); and very vulnerable materials (alluvium, alluvium sand, and limestone crust) (Mihi et al., 2020).

Input data

The most important step for modelling data is to choose the appropriate existing factors that could be adopted in multi criteria decision analysis (MCDA). In our study, it is almost impossible to consider the entire database for the establishment of the sensitivity map because the criteria involved in the wind erosion phenomenon are innumerable and make its modelling very delicate, as well as, availability of input required data to use in the model represents also a limiting factor in the multi criteria analysis process. To overcome the problem of data scarcity, it is necessary to select only the relevant criteria for the analysis. To address these needs, the contributing factors chosen to wind erosion hazard modelling include anthropic pression, soil proprieties, physical environment (vegetation cover, and extent of sand movement), and climatic parameter (wind speed and aridity index). The data used in this study were collected from multi-source datasets (remote sensing images from satellites), existing digitized data in the form of GIS vector maps, government statistical data, and data from the past studies or field surveys of the study area: (1) Four Landsat 8 OLI images were used to build mosaic image for the year 2014 (path/row 192/35, 192/36, 28/45, 193/35 and 193/36) with a spatial resolution of 30 m. All four images were acquired in august month because cloud cover (CC) is less important

during summer period (CC< 2%). According to Afrasinei et al. (2017), only Landsat image with less than 10% CC can be used in such study. All Landsat images were sourced from the USGS Landsat archive (L1T) available at http:// glovis.usgs.gov; (2) Shuttle Radar Topography Mission (SRTM) data were used to extract the slope, at 1arc-second resolution (30m) (http://gdem.ersdac.jspacesystems.or.jp); (3) total annual precipitation (mm) and mean annual evapotranspiration (mm) at ~5-km-pixel resolution for 10 years (2009–2018) obtained from the FAO Water Productivity Open-access portal (WaPOR version2) available at https://wapor.apps.fao.org;(4) characteristics of the soil, namely, clay percentage silt percentage, sand percentage, organic matter content were acquired from the Soil grid database (http:// soilgrids.org/); (5) mean wind speeds (m/s) for the period 2008-2017 were downloaded from the Global Wind Atlas website (http://globalwindatlas.info); (6) statistical data on population, agriculture, and grazing during the year 2015 were compiled from directorate general for agriculture (DGA), and spatial planning department (SPD) . All raster parameters cited above were resampled according to the 30× 30 m pixel resolution, and vector layers were prepared at a scale of 1:60,000 (equivalent to 30-m resolution), then converted from vector to raster. Then, all thematic layers were projected to the Universal Transverse Mercator (UTM) Projection zone 32 north with the datum World Geodetic System (WGS) 1984. Since input data has an accumulated effect, the factor that negatively correlated with the others factors must be inversely regrouped.

Calibration

Radimetric calibration (radiometric normalization) is essential step to produce homogeneous multitemporal Landsat datasets. For that reason, Top-Of-Atmosphere (TOA) reflectances was a simple radiometric correction procedure with good results (Vicente-Serrano et al., 2008). To do this, a precise conversion of the DN values to TOA reflectance for OLI bands is possible using the reflectance rescaling coefficients provided in the product metadata file of OLI band data (Zanter, 2016). In the first step, TOA reflectance without sun angle correction was computed using the following equation (formula (1)):

$$p\lambda' = M_P * Q_{cal} + A_p \quad (1)$$

Where: ρλ' =TOA planetary reflectance, without correction for solar angle. Note that Pλ' does not contain a correction for the sun angle, Mρ= band-specific multiplicative rescaling factor from the metadata, Ap= band-specific additive rescaling factor from the metadata, Qcal = quantized and calibrated standard product pixel values [DN]. In the second step, TOA reflectance corrected for the sun angle (Formula (2)):

$$p\lambda = p\lambda' / \cos(\theta_{SZ}) \quad (2)$$

Where: ρλ = TOA planetary reflectance, θSE = local sun elevation angle. The scene centre sun elevation angle in degrees is provided in the metadata, θSZ =local solar zenith angle where; θSZ= 90° − θSE.

Preparation of data layers

Anthropic pressure on the steppe environment (APSE)

A long history, increase of anthropic pressure has triggered the accentuation of wind erosion processes in semiarid and arid region over the world. Here, extention of crops, excessive tillage, overgrazing, misuse of water resources, deforestation (wood cutting) can be directly destroyed the natural vegetative and hence accelerated wind erosion, therefore, human activities are one of major factors in wind erosion risk assessment (Ge et al., 2015). The parameters used to determine APSE in this study are distance to urban area (DUA), distance to roads (DR), slope gradient (SG), Livestock density (LD), Population density (PD), and Farmland presence (FP). All the mapped inputs data ware reclassified according human impact characteristics. Meanwhile, areas having more anthropic pressure are considered as optimal for wind erosion occurrence.

1. Distance to urban area and to roads**:** urban area and road network were obtained by digitization of Landsat image. After rasterization, Euclidean distance method was applied (Distance module in IDRISI Kilimanjaro GIS software) to compute distance to urban area (DUA) and to roads (DR) (Table 5). DUA are grouped into 4 classes, namely: very close (<500); close (500-1000); nearby (1000-1500); and distant (>1500m).While, four buffer classes are defined at 150-m interval for DR parameter: very close (<150); close (150-300); nearby (300-350); and distant (>350m). Generally, anthropic pressure decreases with increasing distance to urban area and to roads.

2. Slope gradient*:* slope degree map was prepared from the DEM and classified into four different classes as shown in Table 5: nearly level (< 5); (2) gently sloping (6–15); (3) strongly sloping (16–35); and (4) steep to very steep (> 35°). Overall, areas with a less than 5 ° slope are more favourable human activity and areas where the land slope is greater than 35° are considered to be less vulnerable to anthropic disturbs.

3. Livestock, and population density, farmland presence**:** data about farmland, livestock number (sheep, cattle, camelin, and goat), and population number for the 28 municipalities in the study area were collected from official sources (directorate general for agriculture, and spatial planning department). LD, PD, and DP area calculated by dividing the farmland, number of

population, and number of livestock by the study area, respectively (Table 5). An index varying from 1 to 4 is assigned to each factor such as; Livestock density: low (0.21-0.39), medium (0.39-1.17), high (1.17-1.47), and very high (1.47-4.79 head/km^2); Population density: low (0.03-0.11), medium (0.11-0.38), high (0.38-0.73), and very high (0.73-9.98 People / km^2); farmland presence: low (0.04-0.16) , medium (0.16-0.44), high (0.44-0.54), and very high(0.54-0.87). To conclude, areas corresponding to farmland, with high overgrazing, and high population growth were considered the worst type of anthropic activities.

Soil erodibility (SE)

Soil erodibility represent a crucial tache in understanding the potential of soils particles to be transported by wind (Webb and Strong, 2011). Wind erosion is widely controlled by the presence or absence of soil erodible particles (Mirmousavi, 2016). In this research study, four parameters were used to define the soil erodibility factor; clay, silt, sand, and organic matter content. These parameters are typically the most important ones related to soil erodibility. To ensure that all fractions were rescaled between 0 and 100 percent, the present equation developed by Hengl et al. (2017) was applied for clay, silt, sand content as follow (Formula (3)), e.g.:

$$Sand\ (\%)_c = \frac{Sand}{(Sand+Silt+Clay)} \times 100 \quad (3)$$

Where $Sand_c$ (%) is the corrected sand content .Collectively, each one of soil proprieties used in this research were assigned with four classes (Table 5); clay content in percent: low (4-14.72), moderate (14.73-25.46), high (25.47-36.19), and very high (36.20-46.93 %); Silt content percent: low (6.95-15.21), moderate (15.21-23.47), high (23.47-31.74), and very high (31.74-40 %); sand content percent: low (31.70-45.28), medium (45.28-58.85), high (58.85-72.43), and very high (72.43-86 %); organic matter content: low (0-15.63) moderate (15.63-31.26), high (31.26-46.89), and very high(46.89-62.52 %). In short, soil erodibility risk increases with increasing of sand content, and decreases whenever the clay, silt, and organic matter content increasing.

Cover vegetation

Density of vegetation represent the sensitivity of land to wind erosion. Presence of vegetation play an important role in controlling soil erosivity, thereby decreasing the wind erosion. In fact, soil particles held together by plant roots, allowing the accumulation of organic matter (improve soil fertility), and increase soil aggregation (Hong et al., 2020). Baumgertel et

al. (2019) chose Normalized Difference Vegetation Index (NDVI) as good indicator for vegetation cover (VC) detection. The following equation was adopted to calculate the NDVI index (formula 4) (Rouse et al., 1974):

$$\text{NDVI} = \frac{(NIR-R)}{(NIR+R)} \quad (4)$$

Where: NIR = near infrared, R= visible red. NDVI values varied between -1 to +1, in areas of high vegetation density, NDVI was characterized by values of +0.6 to +1, barren soil represented by 0 values, whereas water corps have a negative values (Weng, 2010). Four classes of VC were distinguished according to their contribution degrees to wind erosion (Table 5): (1) water corps (-0.71-0), desert steppe (0-0.15), steppe (0.15-0.30), and forest steppe (0.30-0.88). In the present study, desert steppe was considered the worst type of vegetation cover for wind erosion risk, followed by steppe, and after that forest steppe.

Extent of sand movement

According to Shi et al. (2004), the most severe erosion found in areas of sand dunes and sand accumulation decreased as altitude increased, and increased whenever the wind velocity decreased. In fact, the crust index (CI) is useful for mapping and detecting soils crusts, and to discriminate between different sand dune environment, bare soil, and other soils types (Mihi et al., 2018; Mihi et al., 2019). CI index was computed based on the following equation (formula 5):

$$CI = 1 - \left(\frac{(R-B)}{(R+B)}\right) \quad (5)$$

Where: R = blue band, B= red band. CI values changed typically between 0 and 2. Values close to 0 indicate unconsolidated soil (active and mobile sand dunes), whereas values close to 2 represent stable and consolidated soil (Karnieli, 1997). Starting from CI, four lithologic/morphologic units can be defined in the study area (Table 5): unconsolidated soil (Active and mobile sand movement) (0.62-0.71), physical crust (0.71-0.78), biological crust (0.78-0.94), and crust cover (0.94-1.41). Clearly, unconsolidated soil class is most vulnerable to wind erosion, while biological crust is the less vulnerable to the phenomenon.

Wind speed

Wind speed, of course, is the major driving forces for wind erosion phenomenon (Lyles, 1988). In reality, threshold of wind speed is about 6 m/s, but generally changes depending on size and density of material (Skidmore, 1986). Based on Beaufort scale (Ltd, 2001), wind speed map is ordered at scale form 1 to 4 base (Table 5): light breeze (1.06-3.40), gentle breeze (3.40-

5.50), moderate breeze (5.5-8.00), and fresh breeze (8.00-11.43 m/s). So, areas with high wind velocity are more vulnerable to wind erosion and vice versa.

Aridity Index (AI)

Mirmousavi (2016) noted that soil moisture decreased with the increase of drought, which is translated as increase in wind erosion risk. In this current study, Aridity Index (AI) was opted as a drought indicator and combined with other variables to create a wind-erosion hazard map (Becerril-Pina et al., 2015). AI is given by the following relationship (formula 6).

$$AI = \frac{P}{ETP} \quad (6)$$

Where *P* is total annual precipitation in mm and *ETP* is mean annual evapotranspiration in mm, where AI climatic classification is a unitless values and varies from 0 to 1 (UNEP, 1992). In this present study, AI is reclassified in two classes or climates (Table 5): Arid (0.06-0.2), Semi-arid (0.2-0.35). Therefore, it is generally accepted that wind erosion frequency increases in dry or arid areas.

Methodology

Application of analytical hierarchy process (AHP)

The methodological workflow of the study is summarized as a flowchart in Fig. 2. Thomas Saaty introduced the AHP method in the 1970s, to decompose the problem into a multi-level hierarchical structure of objectives, criteria, sub criteria, and alternatives using pairwise comparison (PCM). In this paper, AHP approach was adopted to: (i) determine the influence of anthropogenic pressures on land degradation in the steppe area (Wilaya of Tebessa) using six factors cited above, and (ii) assess soil erodibility susceptibility starting from four parameters as mentioned earlier. Generally, this method is based on three stages (Saaty 1977; 1980); (1) model structuration, (2) determining the relative importance (weight) of each factor, and (3) application of weighted linear combination. In the first step, in order to integrate multiple factors in the model, it should make them comparable. To accomplish this task, the factors are standardized on a continuous common from 0 (least suitable) to 255 (the most suitable) through 128 (moderately suitable) as shown in the following equation (Eastman 2006). (formula 7):

$$Y = \frac{(X_i - X_{min})}{(X_{max} - X_{min})} \times \text{standarized range}, \quad (7)$$

Where Y is the normalized value of each variable, and Xi, Xmax, and Xmin are actuel value, maximum and minimum values observed in all actual measurement, respectively. In the second step, for the weighting of the criteria we used the approach called pairwise comparisons. Their importance is determined on a numerical scale of 9 levels (Table 1); 1(equal importance) to 9 (extremely more important). Reciprocals values used for the inverse relationship. Comparisons refer to the relative importance of each factor with respect to another to determine its weight. In this way, the importance of each factor is determined by the weight that it is assigned, whose sum of weights equals one. Pairwise comparison of n criteria is given in an evaluation matrix (n*n) as shown in the following equation formula 8):

$$A = \begin{bmatrix} a_{11} & a_{12} & \cdots & a_{1n} \\ a_{21} & a_{22} & \dots & a_{2n} \\ \vdots & \vdots & \ddots & \vdots \\ a_{n1} & a_{n2} & \dots & a_{mn} \end{bmatrix} a_{ii} = 1, a_{ji} = {}^{1}/_{a_{ij}}, a_{ij} = \frac{w_i}{w_j} \quad (8)$$

Where, A represent judgment matrix, wi means weight for attribute ‘i’, wj means weightfor attribute ‘j’. This step is very delicate and depends mainly on nature of the problem to be treated, cultural, personality context of the judgment, and the scientific environment in which the approach will be conducted. By doing so, questionnaires were provided to 30 experts (technicians, engineers, professors, PhD students, decision makers, and specialist is steppe region and climate science) were selected heterogeneously from universities, research institutions, government agencies; directorate general of forest (DGF), directorate general for agriculture (DGA), and high commission for the development of steppe (HCDS). In this connection, a decision-maker must "weigh" several options before deciding on one of them, taking into account a series of criteria, which he considers more or less essential to respect. The weighting values are calculated using the WEIGHT module integrated in the IDRISI Kilimanjaro GIS software. To conclude, pairwise comparison matrix determining factor weights are illustrated in Table 4**.** The quality of AHP outputs strongly depends the consistency between expert opinions. Here, the consistency index (CI) and consistency ratio (CR) were used to assess the consistency of judgments as follows (Formulas (9) and (10)):

$$\mathrm{CI} = (\lambda_{\max} - \mathrm{n})/(\mathrm{n} - 1) \quad (9)$$

$$\mathrm{CR} = \mathrm{CI}/\mathrm{RI} \quad (10)$$

Where λmax and n are the largest eigenvalue and order of matrix, respectively. RI is the Random Index depending on the order of the matrix given by Saaty (1980) as displayed in Table

2**.** CR changes from 0 and 1. If the CR index is greater than 0.10, the preference matrix should be revised. In this present study, CR_{APSE}, CR_{SE}, and CR_{FWER} equals to 0.02, 0.02, and 0.03, respectively, expressing a satisfactory consistency of judgments (Table 4).

Application of fuzzy analytical hierarchy process (FAHP)

In fact, Zadeh (1965) firstly introduced fuzzy logic and its basic idea is to consider the spatial objects on a map as members of a set to deal with ambiguities and uncertainties that usually exist in human judgment. In prior research, fuzzy logic represent a powerful approach, which is characterized by a degree of vagueness and uncertainty, and can be easily incorporated with a GIS modelling language. In reality, FAHP approach is an extension of the AHP method, and since the AHP, method depends on the use of traditional crisp numbers (e.g., 1, 2…9), and vagueness is an essential characteristic of expert problems. In this connection, FAHP method has been developed to constructed final wind erosion map based on six factors: anthropic pressure, soil erodibility, vegetation cover, extent of sand movement, wind speed, and AI. Characteristically, FAHP method is similar to the humans thinking way when dealing with approximate and unconfirmed criteria to make decisions. Furthermore, it maintains the basic characteristics of the AHP method. Up to now a different approach of FAHP have been proposed in prior research using linear, S-curve, triangular, or trapezoidal representations. However, Buckley (1985) developed a new model by using trapezoidal fuzzy numbers, which is easy to set up, implement, and understand compared with other commonly used methods (Chou et al., 2019; Mokhtari et al., 2020; Turan et al., 2020). Practically, the fuzzy AHP approach involves three steps, namely construction of a crisp PCM and its fuzzification, determining the weightings of the assessment criteria, and defuzzification and crisp value normalization.

1. Fuzzification: the triangular fuzzy number (TFN) was adopted for converting a real scale value (crisp set) into fuzzy value (fuzzy sets) as summarized in Table 3. In particular, TFN function is simpler, and less complex, and able to deal with fuzzy data (Chou et al., 2019). As it is stated earlier, normalized of all factors used to a common scale of measurement is necessary. Indeed, the fuzzy membership values for each causative factor of wind erosion is standardized between 0 and 1 (min = 0, max = 1), with zero and one represent the worst and best sensibility areas to wind erosion phenomenon for each factor, as given in the previously used equation (formula 7).We define a fuzzy number $\tilde{A}$ on $\mathbb{R}(= (-\infty, +\infty)$ to be a TFN if its membership function $\mu_{\tilde{A}}(x)$: $\mathbb{R} \to [0,1]$ is equal to (formula 11):

$$\mu_{\tilde{A}}(x) = \begin{cases} \frac{x-l}{m-l}, & l \le x \le m, \\ \frac{u-x}{u-m}, & m \le x \le u, \\ 0, otherwies, \end{cases} \quad (11)$$

Where l, m, and u represent the lower, mean, and upper bounds, respectively, of the fuzzy number $\tilde{A}$ as illustrated in Fig. 3 .Consider two triangular fuzzy numbers $\tilde{A}_1$ and $\tilde{A}_2$, $\tilde{A}_1 = (l_1, m_1, u_1)$, and $\tilde{A}_2 = (l_2, m_2, u_2)$. Their operational laws are provided by formulas (12)-(16).

Addition of a fuzzy number $\oplus$

$$\tilde{A}_1 \oplus \tilde{A}_2 = (l_1, m_1, u_1) \oplus (l_2, m_2, u_2) = (l_1 + l_2, m_1 + m_2, u_1 + u_2) \quad (12)$$

Multiplication of a fuzzy number $\otimes$

$$\tilde{A}_1 \otimes \tilde{A}_2 = (l_1, m_1, u_1) \otimes (l_2, m_2, u_2) = (l_1 l_2, m_1 m_2, u_1 u_2) \quad (13)$$

for $l_1 l_2 > 0$; $m_1 m_2 > 0$; $u_1 u_2 > 0$

Subtraction of a fuzzy number $\ominus$

$$\tilde{A}_1 \ominus \tilde{A}_2 = (l_1, m_1, u_1) \ominus (l_2, m_2, u_2) = (l_1 - l_2, m_1 - m_2, u_1 - u_2) \quad (14)$$

Division of a fuzzy number $\oslash$

$$\tilde{A}_1 \oslash \tilde{A}_2 = (l_1, m_1, u_1) \oslash (l_2, m_2, u_2) = (l_1 / l_2, m_1 / m_2, u_1 / u_2) \quad (15)$$

for $l_1 l_2 > 0$; $m_1 m_2 > 0$; $u_1 u_2 > 0$

Reciprocal of a fuzzy number

$$\tilde{A}_1^{-1} = (l_1, m_1, u_1)^{-1} = (1/l_1, 1/m_1, 1/u_1) \quad (16)$$

for $l_1 l_2 > 0$; $m_1 m_2 > 0$; $u_1 u_2 > 0$

2. Determining the weightings of the assessment criteria: fuzzy judgment matrix using the triangle fuzzy number values (Table 4) are constructed between all criteria in the hierarchical structure instead the constant pairwise comparison values in the classical AHP method as follow (formula 17):

$$\tilde{A} = \begin{bmatrix} \tilde{a}_{11} & \tilde{a}_{12} & \cdots & \tilde{a}_{1n} \\ \tilde{a}_{21} & \tilde{a}_{22} & \cdots & \tilde{a}_{2n} \\ \vdots & \vdots & \ddots & \vdots \\ \tilde{a}_{n1} & \tilde{a}_{n2} & \cdots & \tilde{a}_{mn} \end{bmatrix} \quad (17)$$

Where: $\tilde{A}$ represent n*n-fuzzy judgment matrix containing TFN, $\tilde{a}_{ij} = (l_{ij}, m_{ij}, u_{ij})$, $\tilde{a}_{ji} = 1/\tilde{a}_{ij}$, for $i, j = 1, \ldots, n$ and $i \neq j$, n is the total number of criteria. Afterward, geometric mean method (Buckley, 1985) was used to define the fuzzy geometrical mean and fuzzy weights of each criterion by using the following equation (formula 18, and 19):

$$\tilde{r}_i = (\tilde{a}_{i1} \otimes \tilde{a}_{i2} \otimes \ldots \otimes \tilde{a}_{in})^{1/n} \quad (18)$$

And then, $\widetilde{w}_i = \tilde{r}_i \otimes (\tilde{r}_1 \otimes \ldots \otimes \tilde{r}_n)^{-1}$ (19)

Where $\tilde{a}_{in}$ is the fuzzy value of attribute i with respect to attribute n; so, $\tilde{r}_i$is the geometrical mean of the fuzzy comparison values of attribute i for each criterion n, and $\widetilde{w}_i$ is the fuzzy weight of attribute I and can be noted by a TFN, $\widetilde{w}_i = (lw_i, mw_i, uw_i)$, with lw_i and uw_i represent the lowest and the highest boundaries, respectively, of the fuzzy weighting of the criterion i, and $mw_i$is the modal weight.

3. Defuzzification: defuzzification is a mathematical process of obtaining a single crisp value from the output of the fuzzy set results. The defuzzification of the fuzzy weights of a criterion is done by computing the best non-fuzzy performance (BNP) value of the final weights. The most popular, simple and practical defuzzification method, namely center of area method (COA) (Sun, 2010). The BNP weight wi of the fuzzy weights (lw_i, mw_i, uw_i) can be found based on the following equation (formula 20):

$$\mathrm{BNP}(w_i) = (lw_i, mw_i, uw_i/3) \quad (20)$$

Additive linear model

Overall, two ways to cross the factors, either by considering that the result is the consequence of the interaction between the factors (multiplicative model) or the accumulation of their action (additive model).In the present study, the choice of the additive mode is justified by the fact that the causative factors for wind erosion have effects with each other (Cissokho, 2012). Further, additive model is better fit and easier for both policy maker and scholars to use and understand (Lund, 1995; Choo and Wedley, 2008). The weighted linear combination (WLC) method was used in this work for mapping anthropic pressure on the steppe environment, soil erodibility, and final synthetic wind erosion risk. WLC seems as the most straightforward overlay way, and widely used in GIS decision models (Malczewski, 2006). In this procedure, aggregation by WLC allowed using the full potential of all factors such as continuous areas (formula 21); the values of all factors were multiplied by their corresponding weight in each standardized grid to elaborate the synthetic map, where the weights expresses the relative importance of each factor for the overall objective. Accordingly, maps of anthropic pressure on the steppe environment ($\mathrm{APSE}_{\mathrm{AHP}}$), soil erodibility ($\mathrm{SE}_{\mathrm{AHP}}$), and final wind erosion

462 risk ($FWER_{fAHP}$) were constructed using WLC method using the following equations (formulas
463 22-24).
464 $$C = \sum W_i \times X_i \quad (21)$$
465 Where C is the composite index, Wi and Xi are the weight values and the potential rating of
466 each factor,
467 $$APSE_{AHP} = \big((W_{AHP} \times \text{distance to urban area}) + (W_{AHP} \times \text{distance to roads}) + (W_{AHP} \times$$
468 $$\text{slope gradient}) + (W_{AHP} \times \text{livestock density}) + (W_{AHP} \times \text{population density}) + (W_{AHP} \times$$
469 $$\text{farmland presence})\big) \quad (22)$$
470 $$SE_{AHP} = \big((W_{AHP} \times \text{clay content}) + (W_{AHP} \times \text{silt content}) + (W_{AHP} \times \text{sand content}) + (W_{AHP} \times$$
471 $$\text{soil organic carbon content})\big) \quad (23)$$
472 $$FWER_{fAHP} = \big((W_{fAHP} \times \text{anthropic pressure on the steppe environment}) + (W_{fAHP} \times \text{soil erodibility}) +$$
473 $$(W_{fAHP} \times \text{vegetation cover}) + (W_{fAHP} \times \text{extent of sand movement}) + (W_{fAHP} \times \text{wind speed}) + (W_{fAHP} \times$$
474 $$\text{aridty index})\big) \quad (24)$$
475 Where W_{AHP} and W_{fAHP} were the weightage for each factor using AHP, and FAHP methods,
476 respectively. Finally, each obtained grid map is reclassified into four equal classes—slight,
477 moderate, high, and very high. Equal interval method was adopted by different literature to
478 divide the synthetically final map in hazard naturel assessment (Effat and Hegazy 2014).
479
480 *Validation of the wind erosion susceptibility map*
481 Ideally, prediction without knowing data accuracy and precision are a little use in science.
482 For that reason, sand dunes areas was mapped and checked starting from high-resolution image
483 (Google Earth) and field data verification (Fig. 9a-f). Here, the choice of verification stations
484 were greatly depends on the following criteria including proximity and accessibility in terms of
485 roads, altitude, aspect, security, and data representativeness for the whole of study area. Here,
486 accuracy assessment of the constructed model in its natural context is extremely difficult at this
487 scale, given to scarcity or absence of prior research, high cost and length of the experimentation,
488 in addition to spatiotemporal variability of the wind erosion phenomenon in the region. The
489 validation of wind erosion risk model was achieved by comparing the known sand dunes
490 location data with the wind erosion risk map using Area Under Curve (AUC) method. The AUC
491 method is frequently used to assess the accuracy of the prediction models in natural hazard
492 assessment (Saadoud et al., 2017, 2018). The ROC curve graphs is generated by plotting with
493 respect to the true positive rate (Y-axis) and the false positive rate values (X-axis). In this type
494 of analysis, AUC values fall between 0.5 to 1 noting the rate of goodness. It can be classified
495 into five levels to represent different levels of accuracy: 0.90–1.00 (excellent), 0.80–0.90

(good), 0.70–0.80 (satisfactory), and 0.60–0.70 (poor), and 0.50–0.60 (failing). To that end, the Relative Operating Characteristic (ROC) model in IDRISI Kilimanjaro GIS software was used to compute AUC value.

Results

The DUA, DR, SG, LD, PD, and FP maps (Fig. 4a-f and Table 5) are used to draw the map of anthropic pressure on the steppe environment parameter in Tebessa area. APSE map were grouped into four classes to define areas most exposed to human impact along the study area. The first class corresponds to slight sensitivity, which distributed exclusively in the southern part, occupying 5.18 % of the whole area. The second class belongs to moderate sensitivity, representing 10.28 % of the total area, and located in the south. The third class presents high sensitivity, corresponding to 33.68 % of the entire area. The fourth class represents very high sensitivity, which covered the northern part, with 50.87 % of the study area (Fig.6a and Table 5).

Outs of soil erodibility factor of the study area is illustrated in Fig. 6b and Table 5. Generally, it shows a high erodibility for the majority of research area especially in the south. High erodibility soil class covering approximately one-half (50.87%) of the total area. It is followed by very high erodiblity class with rate of 26.57 %, then Moderate erodiblity class with 18.45 %, and finally slight erodiblity class is poorly represented with 4.42%. The contribution of each four factor in each class of soil erodibility parameter is summarized in Fig. 5a-d and Table 5.

Fig. 6c and Table 5 show that the majority of the vegetation in study area was highly vulnerable to wind erosion since main vegetation consists of desert steppe and steppe with a cover of 52.21 % and 45.37 %, respectively. Very few areas have good vegetation density including forest steppe (2.42 %), and water corps (0.01%). These areas are considered as the less vulnerable, and located in the northern of the study area.

Map of sand movement extent show high sensitivity to wind erosion in the far south of the land area, due to the presence of sandy soils in these areas (Fig.6d and Table 5). Four lithologic/morphologic units were retained along the study area: (1) Physical crust, representing more than one-half of the total area (56.36%) ; (2) Biological crust, with 36.08 %; (3) Unconsolidated soil (Active and mobile sand movement), which represent 4.72 %; and (4) Crust cover with only 2.84 %.

Theoretically, highest intensity of wind speed leading to a highest vulnerability of wind erosion, which occurs mainly in the southeast of the total area. Throughout the study area, wind speeds intensity increase from light breeze (1.06-3.40 m/s), with 21.43 % to gentle breeze (3.40-5.50

m/s), which is almost distributed over three-quarters of the study area with ~ 76.63%, while moderate breeze (5.5-8.00 m/s) are diffused over only 1.92 % of the total area. Fresh breeze (8.00-11.43 m/s) are almost do not exist and poorly represented with less than 1% (0.01%) of the total region.

Fig.6f and Table 5 depicts AI for 10 years (2009–2018). In general, wind erosion increase with decreasing in water availability in a region. In short, dryness increase from the north to south in the study area. The results indicate that almost the whole region of Tebessa is classified as "Arid" with 63.08% ,except the north of study area, which are classified as "Semi-arid" with rate of 36.92%.

Vulnerability maps of causal factors were obtained based on the above-described relations. These maps (Figures 6a-f and Table 5) illustrate the spatial distribution of the sensibility of each single parameters contributing to wind erosion phenomenon. The next step, all factors were driven together for the assessment of the environmentally sensitive areas to wind erosion of the entire research area. Fig. 7 and Table 5, clearly shows a high wind erosion risk for the entire research area. Certainly, it appear clear that wind erosion risk intensity varies from area to another in the whole tebessa region, depending on the impact of each six factors, which controls the wind erosion processes. Characteristically, wind erosion severity increase gradually from north to south of the whole tebessa region. Areas of very high sensitivity dominate almost of the total area with 40.22%, whereas, areas of moderate sensitivity diffused over 25.83 % of land area. Elsewhere, areas with high sensitivity, stretching over 24.30% in the middle of the whole research area. Areas of slight sensitivity are poorly represented, and spreads exclusively at the mountainous regions in the far north of region with not more than 10 % (9.65%). The AUC value of ROC curve for present model used is equal to ~96% (Fig. 8), which is considered as an excellent result for the current wind erosion risk map.

Discussion

AHP and FAHP were applied in this current dissertation to model wind erosion risk in Wilaya of Tebessa (Algeria) using six main contributing factors described previously—anthropic pressure on the steppe environment (distance to urban area, distance to roads, slope gradient, livestock density, population density, and farmland presence), soil erodibility (clay, silt, sand , and soil organic carbon content), cover vegetation, extent of sand movement, wind speed intensity, and aridity index for assessing the wind erosion hazard in arid to semiarid area. Similar results were reported in many studies in the Algerian saharan atlas region (Houyou et al., 2016; Bouarfa and Bellal, 2018; Saadoud et al., 2017:2018; Louassa et al., 2018), North

Africa (Malaki et al., 2009; Afrasinei et al., 2018 ; Gómez et al., 2018) and other arid, and semiarid regions around the world (Mirmousavi, 2016; Baumgertel et al., 2019), which indicate that wind erosion vulnerability increase from north to south, refereeing to the effect of related factors which encourage wind erosion— human impact, degrades soil structure, denudation of natural vegetation, extent of sandy soils, and harsh climatic conditions.

Wind erosion is noticeably low in the far north of study area. This is because of the good status of vegetation cover in the form of protective forest belts (dominated by *Pinus halepensis* Mill), good climatic conditions, and less human activities in these few areas localised in the north (Hong et al., 2020). According to Shi et al. (2004), wind erosion risk can be greatly controlled when vegetation cover changed between 40-50%, as well as the plant roots increase the resistance of soils against wind erosion, allowing the accumulation of organic matter, and hence increase the soil aggregation (structural stability) (Zamani and Mahmoodabadi, 2013). Furthermore, mountains with high relief conditions (slopes gradient >35%) play a key role as barrier against the prevailing winds in the study area (Saadoud et al., 2017, 2018).

Wind erosion remains moderate in the north part. This part is characterized by a semi-arid climate, moderate wind intensity, favourable soil structure, absence of anthropogenic activities, and relatively dense vegetal cover. In essence, when the vegetation cover is less than 35%, wind intensity is deemed as the main agent for wind erosion (Bensaïd, 2006). In reality, wind speed velocity increase with increasing of the vertical distance from the soil surface and vice versa (Song et al., 2006). In most cases, wind erosion risk increased as the wind speed, and evapotranspiration increased, while amount of precipitation deceased (≤300mm annually) as stated by Blanco and Lal (2008).

The area of high wind erosion hazard occurs mainly at the plane morphologies, which is characterized by scattered steppe plant communities, such as chamaephytic (represented by *Artemisia herba-alba* Asso, *Artemisia campestris* L), and halophytic (dominated by *Atriplex halimus* L and *Salsola vermiculata* L), (Mihi et al., 2020). Unfortunately, since the early 1980s, steppe vegetation have witnessed a drastic regression, as result of overgrazing, drought (dry climate), and extent of dryland farming (Bensaïd, 2006). Meanwhile, plouwing soil for the conversion of rangeland into cropland make the soil unprotected without any vegetation (barley soil) and triggered its vulnerability to wind erosion processes (Benaradj et al., 2020).

Areas records very high wind erosion risk occurs within the very low elevation area in far south part of the study area**.** This is due to the presence of sand deposits and sandy soils, and the prevailing of erosive winds. In most cases, many plant species were buried under sand masses and replaced gradually by sand dunes vegetation taxa such as psammophytic communities

(Mihi et al., 2019).Obviously, rates of wind erosion increase in order of: humid> dry subhumid> semiarid>arid areas as informed Blanco and Lal (2008). Further, wind erosion severity is mostly recorded in spring season, especially when wind speed exceeds a certain threshold (Song et al., 2006). Additionally, in order to move soil particles by wind, the latter must be reaches 8m/s, at 2m above soil surface. Otherwise, wind speed can be displaced any particles soil less than 1 mm (Brooks et al., 2012). Under these conditions, rates of wind erosion increase, with decreasing in particles sizes: clay>silt> sand (Zheng, 2009).

In the past, in order to fight against sandy desertification, Algeria has launched the largest afforestation program (green dam), which was initiated in 1972. This shelterbelt aimed for the restoration of the ecological balance in arid and semi-arid areas. It represents a band of 1000 Km in long, stretching from the Moroccan border in the west to the Tunisian border in the east, over 20 km in wide (Kepner et al., 2006). As a result, green dam contributed to the accelerated greening trend in the pre-Saharan areas with only 42% during the last twenty years (Bensaïd, 1995). Besides, despite the numerous studies carried out in most regions affected by wind desertification, these studies remain insufficient and do not allow knowing for accurately and comprehensively the impact and consequences of this phenomenon. However, these traditional methods still costly, tedious and the most time-consuming, especially when it's apply over large surface region. Moreover, this old method are performed in a punctually manner which requires mathematical procedures such as interpolation in order to obtain zonal information.

The methodology proposed by this current study is a significant contribution to generalize the wind-erosion risk assessment especially at steppe regions. Furthermore, the proposed approach based on medium resolution satellite data available free is considered to be cost-efficient, simple, and easily to apply for monitoring wind erosion risk. Although the method applied in this work, show an excellent performance accuracy with 96 %. Nevertheless, the results obtained by this study requires future studies that are more detailed with further field measurements at small-scale level for better characterisation of diagnostic criteria and by incorporating additional data such as soil wetness, aerodynamic roughness length, landforms, windbreaks, etc.

Conclusion

This study has estimated the wind erosion hazard in wilaya of Tebessa (northeastern Algeria) using WLC algorithm with AHP, FAHP, and geomatics approaches. The AUC value of ROC curve for the proposed approach was 0.96. This result indicates that proposed model is excellent estimator of wind erosion vulnerability in such regions. In total, wind erosion

vulnerability varying increasingly along a north-to-south gradient of the whole land area. Through this study, it was found that area with; slight, moderate, high, and very high erosion occupied 9.65 %, 25.83 %, 24.30 %, and 40.22 %, respectively, of the entire research area. The free available multi-source remote sensing datasets (medium resolution satellite data) offers an effective opportunity for assessing the hazard magnitude of wind erosion, especially, under data-scarce or areas of difficult access (inaccessible areas) in developing nations. Besides, the obtained thematic map of wind erosion hazard provides a general overview of this phenomenon, which represent an essential tool for decision-makers and planners to develop the successful strategies to control sustainably sand desertification.

References

Afrasinei, G. M., Melis, M. T., Arras, C., Pistis, M., Buttau, C., & Ghiglieri, G. (2018). Spatiotemporal and spectral analysis of sand encroachment dynamics in southern Tunisia. *European Journal of Remote Sensing*, *51*(1), 352-374. https://doi.org/10.1080/22797254.2018.1439343

Afrasinei, G. M., Melis, M. T., Buttau, C., Arras, C., Pistis, M., Zerrim, A., ... & Jlali, A. (2017). Classification methods for detecting and evaluating changes in desertification-related features in arid and semiarid environments. *Euro-Mediterranean Journal for Environmental Integration*, *2*(1), 14. https://doi.org/10.1007/s41207-017-0021-1

Aïdoud, A., Le Floc'h, É., & Le Houérou, H. N. (2006). Les steppes arides du nord de l'Afrique. *Science et changements planétaires/Sécheresse*, *17*(1), 19-30.

Baltas, E. (2007). Spatial distribution of climatic indices in northern Greece. *Meteorological Applications: A journal of forecasting, practical applications, training techniques and modelling*, *14*(1), 69-78. https://doi.org/10.1002/met.7

Baumgertel, A., Lukić, S., Belanović Simić, S., & Kadović, R. (2019). Identifying Areas Sensitive to Wind Erosion—A Case Study of the AP Vojvodina (Serbia). *Applied Sciences*, *9*(23), 5106. https://doi.org/10.3390/app9235106

Becerril-Pina, R., Mastachi-Loza, C. A., González-Sosa, E., Díaz-Delgado, C., & Bâ, K. M. (2015). Assessing desertification risk in the semi-arid highlands of central Mexico. *Journal of Arid Environments*, *120*, 4-13. https://doi.org/10.1016/j.jaridenv.2015.04.006

Benaradj A., Boucherit H., Merzougui T. (2020) Water Resources, State of Play, and Development Prospects in the Steppe Region of Naâma (Western Algeria). In: Negm A.M., Bouderbala A., Chenchouni H., Barceló D. (eds) Water Resources in Algeria - Part II. The Handbook of Environmental Chemistry, vol 98. Springer, Cham. https://doi.org/10.1007/698_2020_537

Bensaïd, A. (2006). *SIG ET TÉLÉDÉTECTION POUR L'ÉTUDE DE L'ENSABLEMENT DANS UNE ZONE ARIDE: LE CAS DE LA WILAYA DE NAÂMA (ALGÉRIE)* (Doctoral dissertation).

Bensaïd, S. (1995). Bilan critique du barrage vert en Algérie. *Sécheresse*, *6*(3), 247-255.

Blanco, H., & Lal, R. (2008). *Principles of soil conservation and management* (Vol. 167169). New York: Springer.

669 Böhner, J., Schäfer, W., Conrad, O., Gross, J., & Ringeler, A. (2003). The WEELS model: methods, results and
670 limitations. *Catena*, *52*(3-4), 289-308. https://doi.org/10.1016/S0341-8162(03)00019-5
671 Bouarfa, S., & Bellal, S. A. (2018). Assessment of the Aeolian sand dynamics in the region of Ain Sefra (Western
672 Algeria), using wind data and satellite imagery. *Arabian Journal of Geosciences*, *11*(3), 56.
673 https://doi.org/10.1007/s12517-017-3346-9
674 Brooks, K. N., Ffolliott, P. F., & Magner, J. A. (2012). *Hydrology and the Management of Watersheds*. John Wiley
675 & Sons.
676 Buckley JJ (1985) Fuzzy hierarchical analysis. Fuzzy Sets Syst 17(3):233–247. https://doi.org/10.1016/0165-
677 0114(85)90090-9
678 Choo, E. U., & Wedley, W. C. (2008). Comparing fundamentals of additive and multiplicative aggregation in ratio
679 scale multi-criteria decision making. *The Open Operational Research Journal*, *2*(1).
680 Chou, Y. C., Yen, H. Y., Dang, V. T., & Sun, C. C. (2019). Assessing the human resource in science and
681 technology for Asian countries: Application of fuzzy AHP and fuzzy TOPSIS. *Symmetry*, *11*(2), 251.
682 https://doi.org/10.3390/sym11020251
683 Cissokho, R. (2012). Developpement d'un indice de vulnerabilite a l'erosion eolienne a partir d'images satellitales,
684 dans le bassin arachidier du Senegal: Cas de la region de Thies. *Ph. D. Thesis*.
685 Djellab S, Mebarkia N, Neffar S, Chenchouni H (2019) Diversity and phenology of hoverflies (Diptera: Syrphidae)
686 in pine forests (Pinus halepensis Miller) of Algeria. J Asia Pac Entomol 22:766–777.
687 https://doi.org/10.1016/j.aspen.2019.05.012
688 Eastman JR (2006) IDRISI Kilimanjaro: guide to GIS and image processing. Clark Labs, Clark University,
689 Worcester
690 Effat HA, Hegazy MN (2014) Mapping landslide susceptibility using satellite data and spatial multicriteria
691 evaluation: the case of Helwan District, Cairo. Appl Geomat 6:215–228. https://doi.org/10.1007/s12518-014-
692 0137-9
693 Ettoumi, F. Y., Sauvageot, H., & Adane, A. E. H. (2003). Statistical bivariate modelling of wind using first-order
694 Markov chain and Weibull distribution. *Renewable energy*, *28*(11), 1787-1802.
695 https://doi.org/10.1016/S0960-1481(03)00019-3
696 Fryrear, D. W., Saleh, A., Bilbro, J. D., Shomberg, H. M., Stout, J. E., & Zobeck, T. M. (1998). REVISED WIND
697 EROSION EQUATION (RWEQ), wind erosion and water conservation research unit, USDA-ARS.
698 Ge, X., Li, Y., Luloff, A. E., Dong, K., & Xiao, J. (2015). Effect of agricultural economic growth on sandy
699 desertification in Horqin Sandy Land. *Ecological Economics*, *119*, 53-63.
700 https://doi.org/10.1016/j.ecolecon.2015.08.006
701 Gómez, D., Salvador, P., Sanz, J., Casanova, C., & Casanova, J. L. (2018). Detecting Areas Vulnerable to Sand
702 Encroachment Using Remote Sensing and GIS Techniques in Nouakchott, Mauritania. *Remote*
703 *Sensing*, *10*(10), 1541. https://doi.org/10.3390/rs10101541
704 Goudie, A. S., & Middleton, N. J. (2006). *Desert dust in the global system*. Springer Science & Business Media.
705 Gregory, J. M., Vining, R., Peck, L., & Wofford, K. (1999, May). TEAM: The Texas Tech Wind Erosion Analysis
706 Model. In *Sustaining the global farm: selected papers from the 10th International Soil Conservation*
707 *Organization Meeting* (pp. 24-29).

Hagen, L. J. (1991). A wind erosion prediction system to meet user needs. *Journal of soil and water conservation*, *46*(2), 106-111.

Hengl, T., de Jesus, J. M., Heuvelink, G. B., Gonzalez, M. R., Kilibarda, M., Blagotić, A., ... & Guevara, M. A. (2017). SoilGrids250m: Global gridded soil information based on machine learning. *PLoS one*, *12*(2). https://doi.org/10.1371/journal.pone.0169748

Hirche, A., Salamani, M., Abdellaoui, A., Benhouhou, S., & Valderrama, J. M. (2011). Landscape changes of desertification in arid areas: the case of south-west Algeria. *Environmental monitoring and assessment*, *179*(1-4), 403-420. https://doi.org/10.1007/s10661-010-1744-5

Hong Ch., Chenchen L., Xueyong Z., Huiru L., Liqiang K., Bo L., Jifeng Li., 2020. Wind erosion rate for vegetated soil cover: A prediction model based on surface shear strength. Catena. https://doi.org/10.1016/j.catena.2019.104398

Houyou, Z., Bielders, C. L., Benhorma, H. A., Dellal, A., & Boutemdjet, A. (2016). Evidence of strong land degradation by wind erosion as a result of rainfed cropping in the Algerian steppe: a case study at Laghouat. *Land Degradation & Development*, *27*(8), 1788-1796. https://doi.org/10.1002/ldr.2295

Huang, M., Peng, G., Zhang, J., & Zhang, S. (2006). Application of artificial neural networks to the prediction of dust storms in Northwest China. *Global and Planetary change*, *52*(1-4), 216-224. https://doi.org/10.1016/j.gloplacha.2006.02.006

Karnieli, A. (1997). Development and implementation of spectral crust index over dune sands. *International Journal of Remote Sensing*, *18*(6), 1207-1220. https://doi.org/10.1080/014311697218368

Kepner, W. G., Rubio, J. L., Mouat, D. A., & Pedrazzini, F. (Eds.). (2006). *Desertification in the Mediterranean Region. A Security Issue: Proceedings of the NATO Mediterranean Dialogue Workshop, held in Valencia, Spain, 2-5 December 2003*. Springer Science & Business Media.

Kouchami-Sardoo, I., Shirani, H., Esfandiarpour-Boroujeni, I., & Bashari, H. (2019). Application of a Bayesian belief network model for assessing the risk of wind erosion: A test with data from wind tunnel experiments. *Aeolian Research*, *41*, 100543. https://doi.org/10.1016/j.aeolia.2019.100543

Louassa, S., Merzouk, M., & Merzouk, N. K. (2018). Sand drift potential in western Algerian Hautes Plaines. *Aeolian Research*, *34*, 27-34. https://doi.org/10.1016/j.aeolia.2018.07.002

Ltd, R. (2001). Wind energy and the plant engineer. In: Snow, D. A. (Ed.). Plant engineer's reference book. Elsevier, pp 44-1-44-7. https://doi.org/10.1016/B978-075064452-5/50099-7

Lund, E. (1995). Comparison of additive and multiplicative models for reproductive risk factors and post-menopausal breast cancer. *Statistics in medicine*, *14*(3), 267-274.

Malaki, A., El Wartiti, M., & El Ghannouchi, A. (2009). Sand dunes evolution and desertification in southeastern Morocco: a new approach to an old problem. In *Desertification and Risk Analysis Using High and Medium Resolution Satellite Data* (pp. 199-206). Springer, Dordrecht. https://doi.org/10.1007/978-1-4020-8937-4_17

Malczewski, J. (2006). GIS-based multicriteria decision analysis: a survey of the literature. *International journal of geographical information science*, *20*(7), 703-726. https://doi.org/10.1080/13658810600661508

Mihi A, Nacer T, Chenchouni H (2018) Monitoring dynamics of date palm plantations from 1984 to 2013 using Landsat time-series in Sahara Desert oases of Algeria. In: El-Askary HM et al (eds) Advances in remote

sensing and geo informatics applications. Springer Nature, Switzerland, pp 225–228. https://doi.org/10.1007/978-3-030-01440-7_52

Mihi A, Tarai N, Chenchouni H (2019) Can palm date plantations and oasification be used as a proxy to fight sustainably against desertification and sand encroachment in hot drylands? Ecol Indic 105: 365–375. https://doi.org/10.1016/j.ecolind.2017.11.027

Mihi, A., Benarfa, N., & Arar, A. (2020). Assessing and mapping water erosion-prone areas in northeastern Algeria using analytic hierarchy process, USLE/RUSLE equation, GIS, and remote sensing. *Applied Geomatics*, 1-13. https://doi.org/10.1007/s12518-019-00289-0

Mirmousavi, S. H. (2016). Regional modeling of wind erosion in the North West and South West of Iran. *Eurasian Soil Science*, *49*(8), 942-953. https://doi.org/10.1134/S1064229316080081

Mokhtari, M., Hoseinzade, Z., & Shirani, K. (2020). A comparison study on landslide prediction through FAHP and Dempster–Shafer methods and their evaluation by P–A plots. *Environmental Earth Sciences*, *79*(3), 76. https://doi.org/10.1007/s12665-019-8804-0

Panagos, P., & Katsoyiannis, A. (2019). Soil erosion modelling: The new challenges as the result of policy developments in Europe, 19 (172), 470-474. https://doi.org/10.1016/j.envres.2019.02.043

Ravi, S., D'Odorico, P., Breshears, D. D., Field, J. P., Goudie, A. S., Huxman, T. E., ... & Van Pelt, S. (2011). Aeolian processes and the biosphere. *Reviews of Geophysics*, *49*(3). https://doi.org/10.1029/2010RG000328

Rouse, J.W., Haas, R.W., Schell, J.A., Deering, D.H., Harlan, J.C., 1974. Monitoring the Vernal Advancement and Retrogradation (Greenwave Effect) of Natural Vegetation.NASA/GSFC, Greenbelt, MD.

Saadoud, D., Guettouche, M. S., Hassani, M., & Peinado, F. J. M. (2017). Modelling wind-erosion risk in the Laghouat region (Algeria) using geomatics approach. *Arabian Journal of Geosciences*, *10*(16), 363. https://doi.org/10.1007/s12517-017-3139-1

Saadoud, D., Hassani, M., Peinado, F. J. M., & Guettouche, M. S. (2018). Application of fuzzy logic approach for wind erosion hazard mapping in Laghouat region (Algeria) using remote sensing and GIS. *Aeolian research*, *32*, 24-34. https://doi.org/10.1016/j.aeolia.2018.01.002

Saaty TL (1977) A scaling method for priorities in hierarchical structures. JMath Psychol 15:234–281. https://doi.org/10.1016/0022-2496 (77) 90033-5

Saaty TL (1980) the analytical hierarchy process. McGraw Hill, New York

Seltzer, P. (1946). Le climat de l'Algérie. 1 vol., 219 p. Carbonel Alger.

Shao, Y. (2008). *Physics and modelling of wind erosion* (Vol. 37). Springer Science & Business Media. 451 p

Shapiro, A. F., & Koissi, M. C. (2017). Fuzzy logic modifications of the Analytic Hierarchy Process. *Insurance: Mathematics and Economics*, *75*, 189-202. https://doi.org/10.1016/j.insmatheco.2017.05.003

Shi, H., Gao, Q., Qi, Y., Liu, J., & Hu, Y. (2010). Wind erosion hazard assessment of the Mongolian Plateau using FCM and GIS techniques. *Environmental Earth Sciences*, *61*(4), 689-697. https://doi.org/10.1007/s12665-009-0381-1

Shi, P., Yan, P., Yuan, Y., & Nearing, M. A. (2004). Wind erosion research in China: past, present and future. *Progress in physical geography*, *28*(3), 366-386. https://doi.org/10.1191/0309133304pp416ra

Skidmore, E. L. (1986). Wind erosion climatic erosivity. *Climatic change*, *9*(1-2), 195-208. https://doi.org/10.1007/BF00140536

Song, Y., Yan, P., & Liu, L. (2006). A review of the research on complex erosion by wind and water. *Journal of Geographical Sciences*, *16*(2), 231-241. https://doi.org/10.1007/s11442-006-0212-1

Sun, C. C. (2010). A performance evaluation model by integrating fuzzy AHP and fuzzy TOPSIS methods. *Expert systems with applications*, *37*(12), 7745-7754. DOI 10.1007/s10346-003-0006-9

Tatarko, J., Wagner, L., & Fox, F. (2019). The wind erosion prediction system and its use in conservation planning. Bridging Among Disciplines by Synthesizing Soil and Plant Processes, (bridgingamongdi). https://doi.org/10.2134/advagricsystmodel8.2017.0021

Turan, İ. D., Özkan, B., Türkeş, M., & Dengiz, O. (2020). Landslide susceptibility mapping for the Black Sea Region with spatial fuzzy multi-criteria decision analysis under semi-humid and humid terrestrial ecosystems. *Theoretical and Applied Climatology*, 1-14. https://doi.org/10.1007/s00704-020-03126-2

UNEP, 1992. World Atlas of Desertification. Edward Arnold, London.

Vicente-Serrano, S. M., Pérez-Cabello, F., & Lasanta, T. (2008). Assessment of radiometric correction techniques in analyzing vegetation variability and change using time series of Landsat images. *Remote sensing of environment*, *112*(10), 3916-3934. https://doi.org/10.1016/j.rse.2008.06.011

Webb, N. P., & Strong, C. L. (2011). Soil erodibility dynamics and its representation for wind erosion and dust emission models. *Aeolian Research*, *3*(2), 165-179. https://doi.org/10.1016/j.aeolia.2011.03.002

Webb, N. P., McGowan, H. A., Phinn, S. R., Leys, J. F., & McTainsh, G. H. (2009). A model to predict land susceptibility to wind erosion in western Queensland, Australia. *Environmental Modelling & Software*, *24*(2), 214-227. https://doi.org/10.1016/j.envsoft.2008.06.006

Weng, Q. (2010). Remote sensing and GIS integration: theories, methods, and applications. New York: McGraw-Hill.

Williams, J., Jones, C., Gassman, P., Hauck, L., 1995. Simulation of animal waste management with APEX. Innovat. New Horizons Livestock Poultry Manure Manage. 1, 22–26.

Woodruff, N. P., & Siddoway, F. H. (1965). A Wind Erosion Equation 1. *Soil Science Society of America Journal*, *29*(5), 602-608. https://doi.org/10.2136/sssaj1965.03615995002900050035x

Yang, Z., Gao, X., & Lei, J. (2021). Fuzzy comprehensive risk evaluation of aeolian disasters in Xinjiang, Northwest China. *Aeolian Research*, *48*, 100647.

Yu, G. M., Liu, Y., Yan, Y., & Hu, Y. F. (2011). Soil wind erosion risk assessment in the middle part of Inner Mongolia Plateau during 2000 to 2008. *Scientia Geographica Sinica*, *31*, 1493-1499.

Zadeh, L. A. (1965). Fuzzy sets. *Information and control*, *8*(3), 338-353. https://doi.org/10.1142/9789814261302_0021

Zamani, S., & Mahmoodabadi, M. (2013). Effect of particle-size distribution on wind erosion rate and soil erodibility. *Archives of Agronomy and Soil Science*, *59*(12), 1743-1753. https://doi.org/10.1080/03650340.2012.748984

Zanter, K., 2016. Landsat 8 (L8) Data Users Handbook. LSDS-1574 Version, 2. URL: https://landsat.usgs.gov/documents/Landsat8DataUsersHandbook.pdf (accessed 10.11.17).

Zheng, X. (2009). *Mechanics of wind-blown sand movements*. Springer Science & Business Media.

Figures

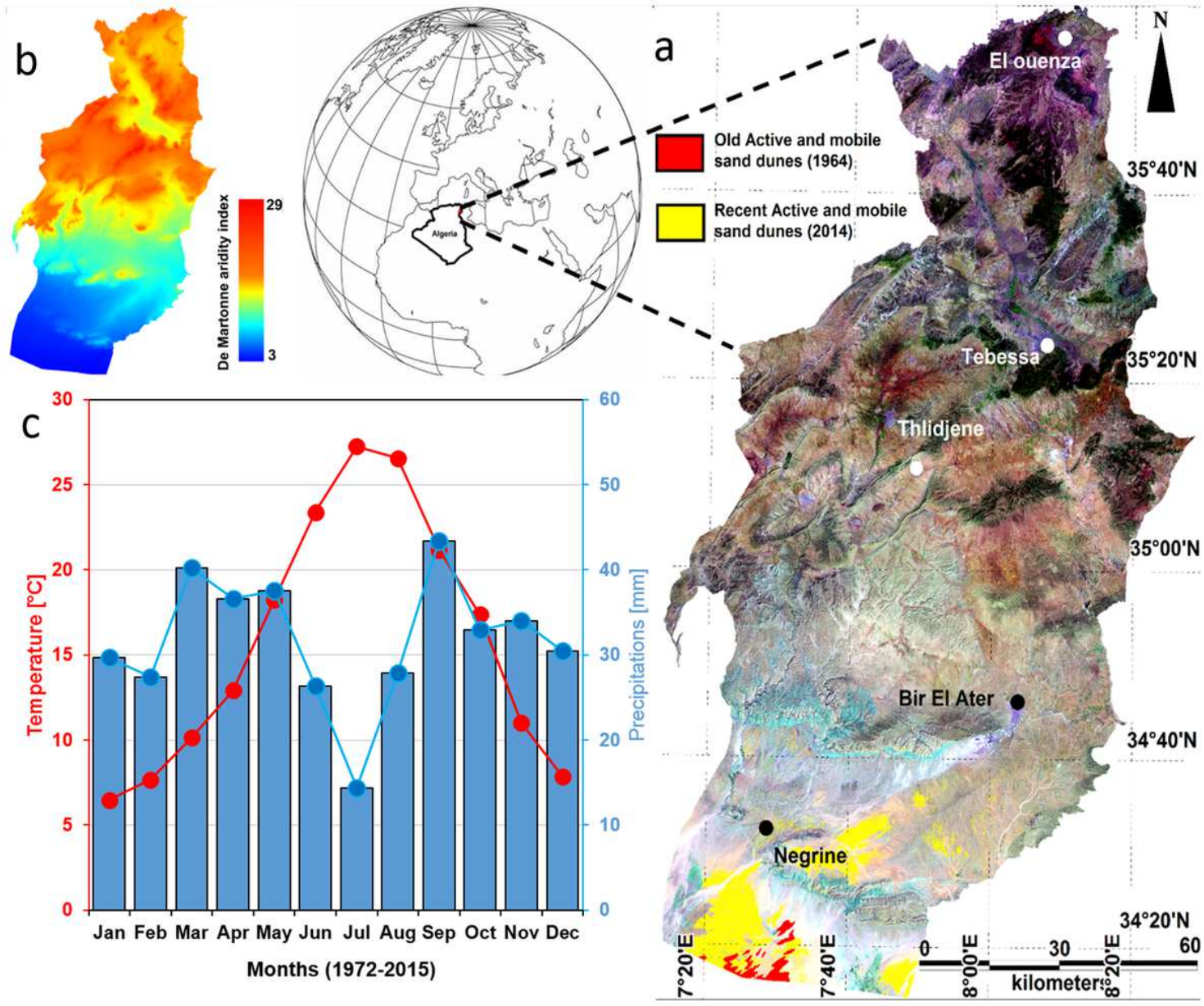


Figure 1

OLI Landsat image of Tebessa region for the year 2014 (RGB composite, Bands 7-5-2), displaying (a) location of the study area, (b) De Martonne Aridity Index in the study area for 50 years (1950–2000) obtained from the World Climate database (http://www.worldclimate.com), (c) ombrothermic diagrams of Gaussen and Bagnouls applied for the period 1972–2015 of the wilaya of Tebessa (Algeria). Note: The designations employed and the presentation of the material on this map do not imply the expression of any opinion whatsoever on the part of Research Square concerning the legal status of any country, territory, city or area or of its authorities, or concerning the delimitation of its frontiers or boundaries. This map has been provided by the authors.

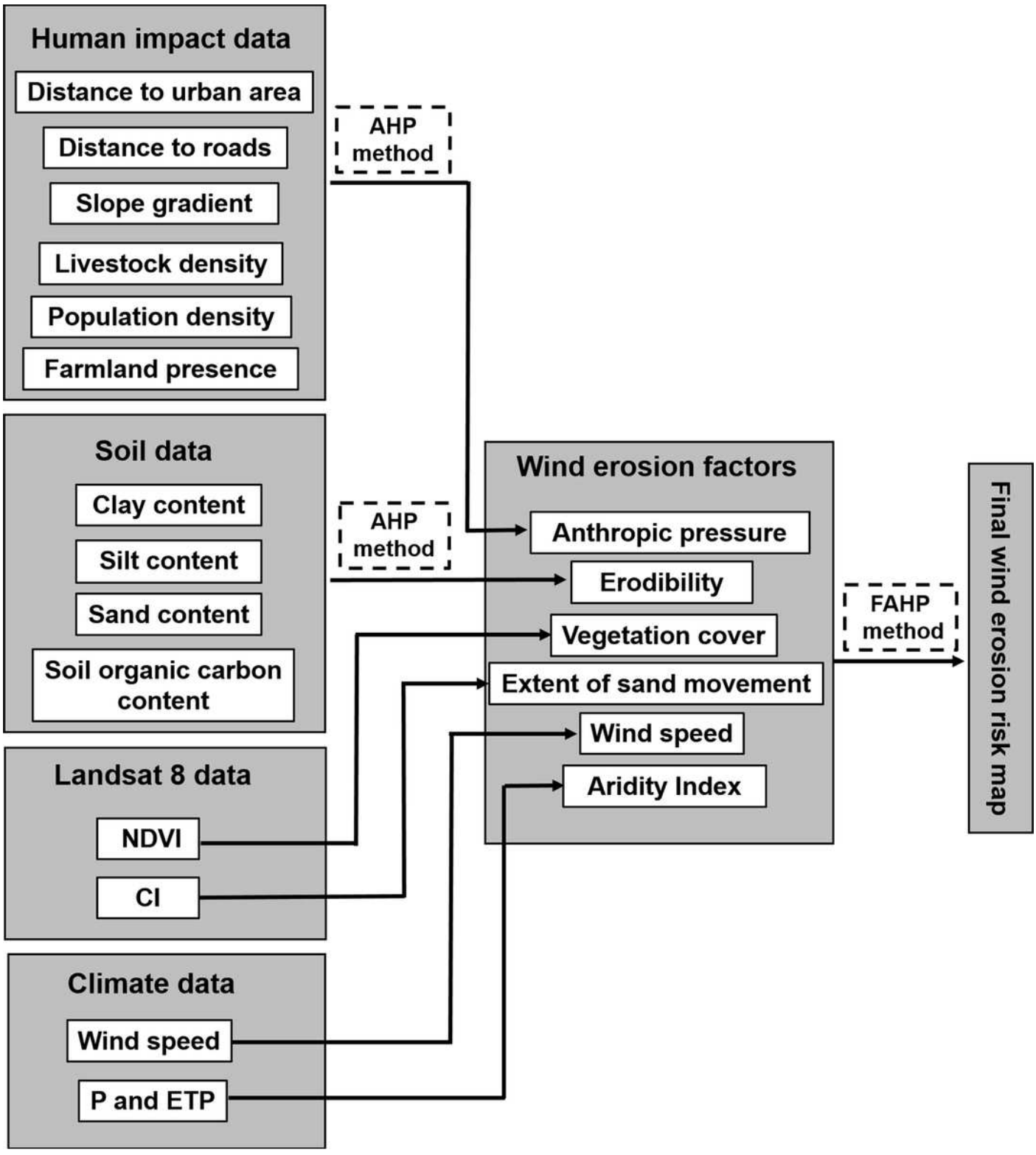


Figure 2

Methodological flowchart applied for mapping wind erosion vulnerability

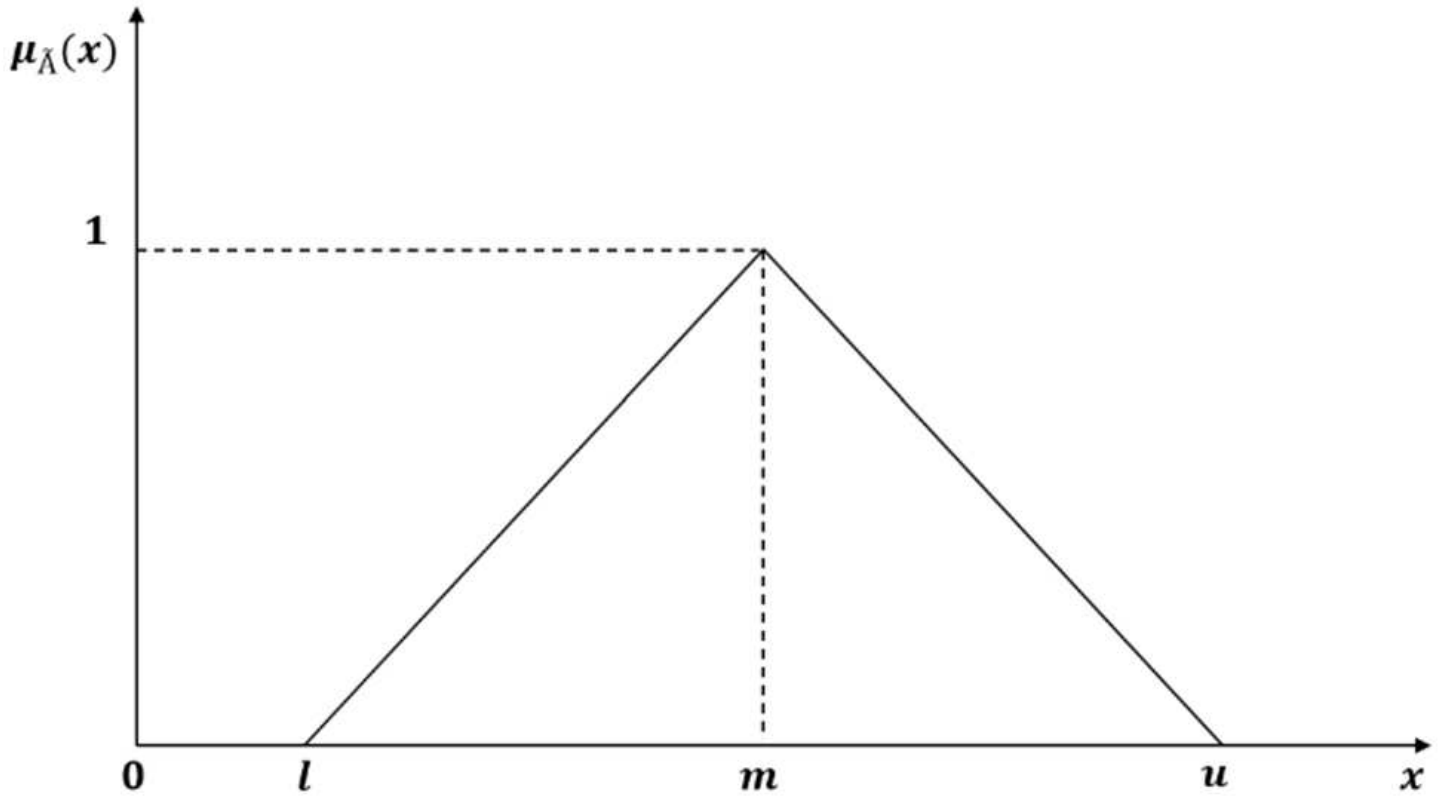


Figure 3

The membership functions of the triangular fuzzy number M = (1, m, u)

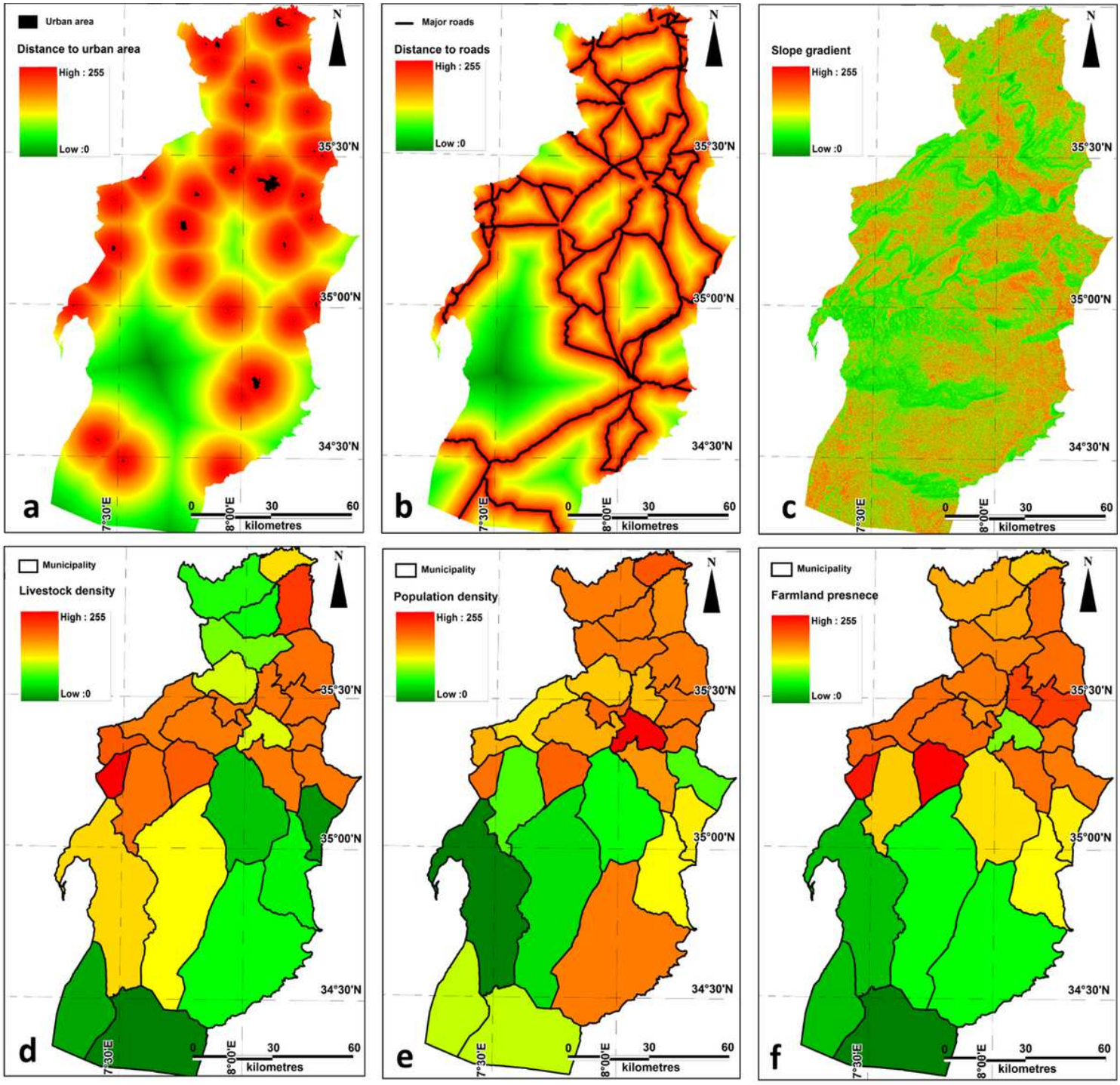


Figure 4

Anthropic pressure affecting factors (a) distance to urban area, (b) distance to roads, (c) slope gradient, (d) livestock density, (e) population density, (f) farmland presence

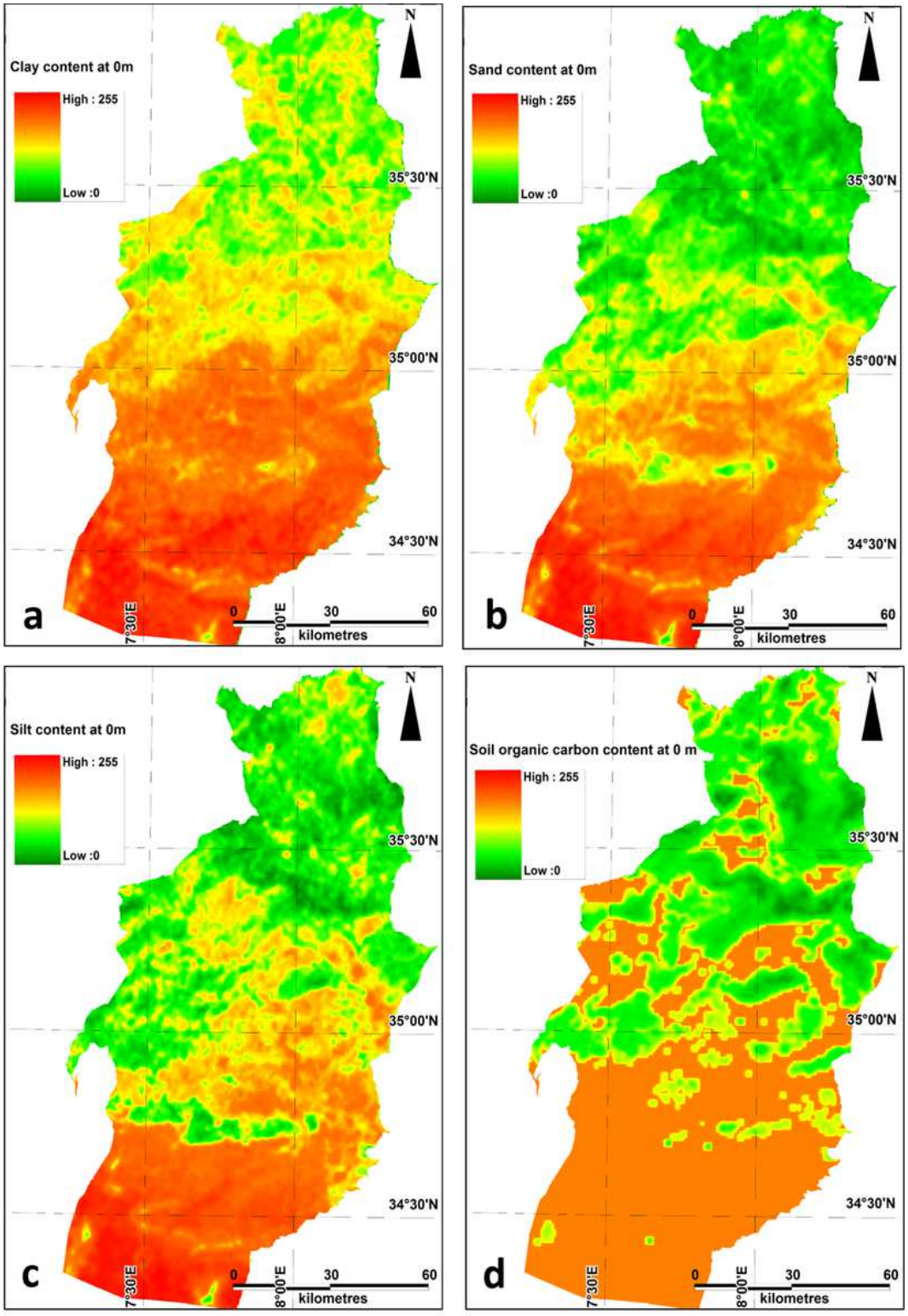


Figure 5

Input data layers used to elaborate soil erodibility factor (a) clay content percent, (b) sand content percent, (c) silt content percent, (d) soil organic carbonic content percent

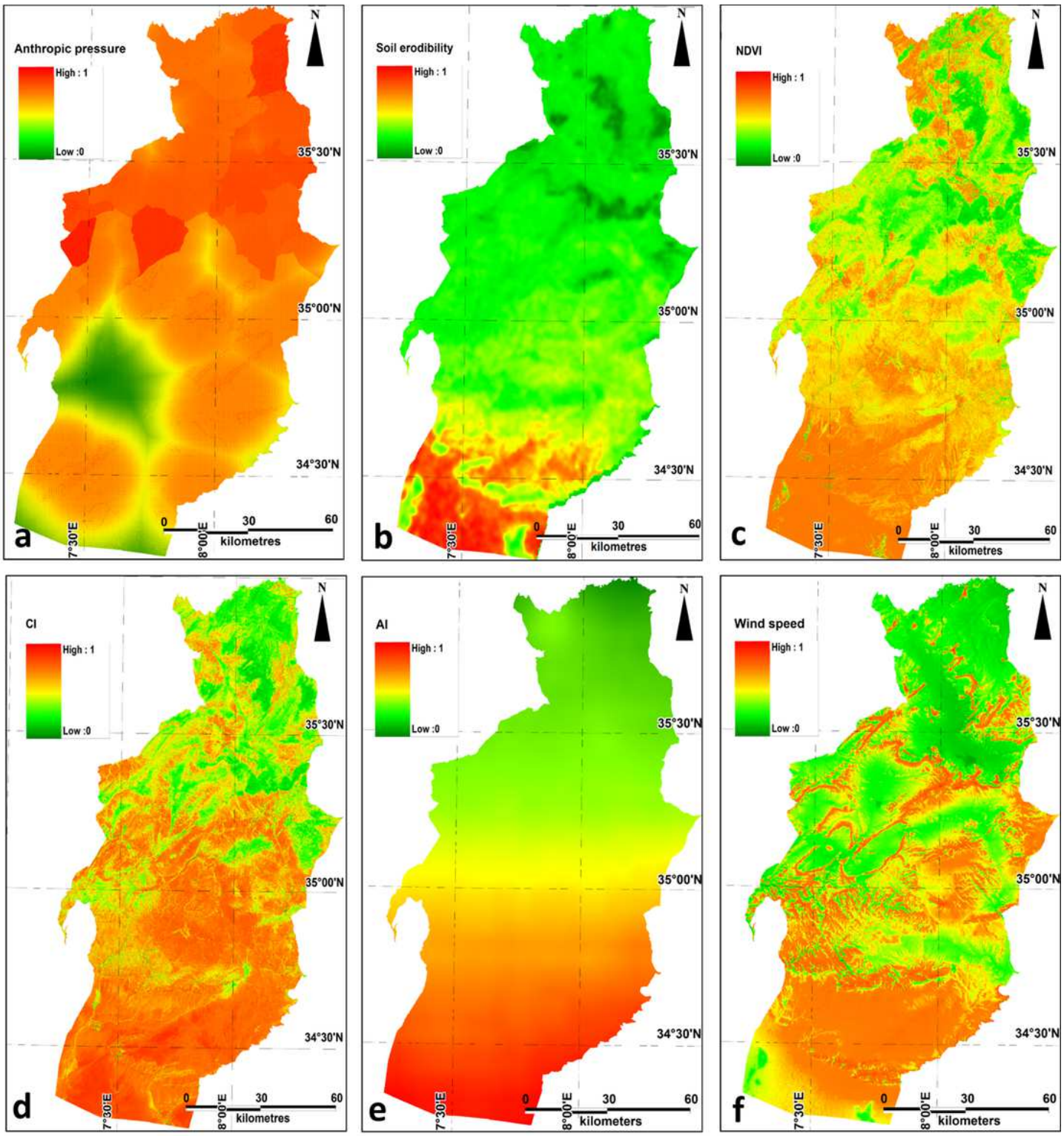


Figure 6

Wind erosion condition factors (a) Anthropic pressure on the steppe environment based on AHP model , (b) soil erodiblity derived from AHP model, (c) Normalized Difference Vegetation Index (NDVI), (d) Crust Index (CI), (e) Aridity Index (AI), and (f)Wind speed

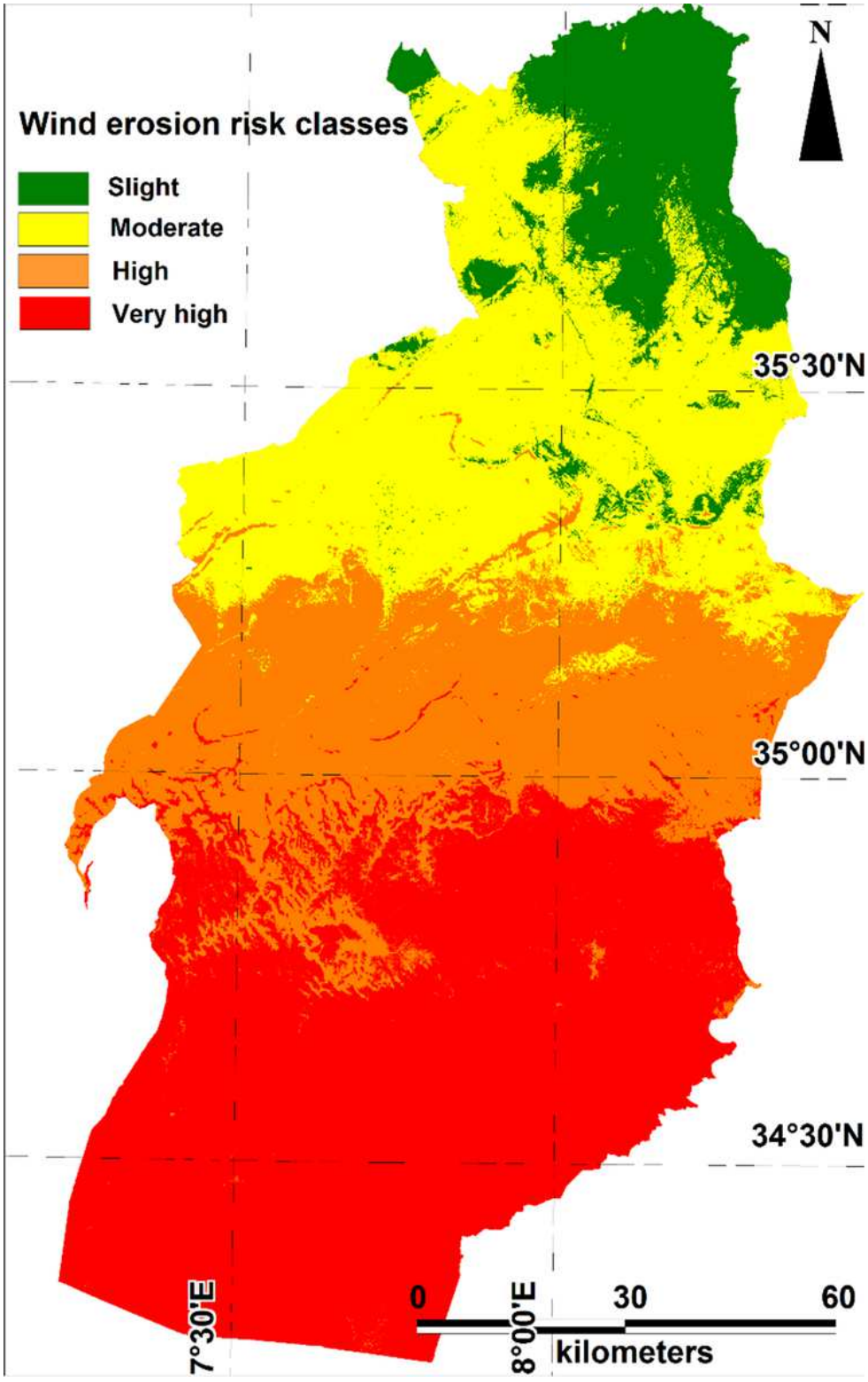


Figure 7

Wind erosion risk map produced by fuzzy logic model

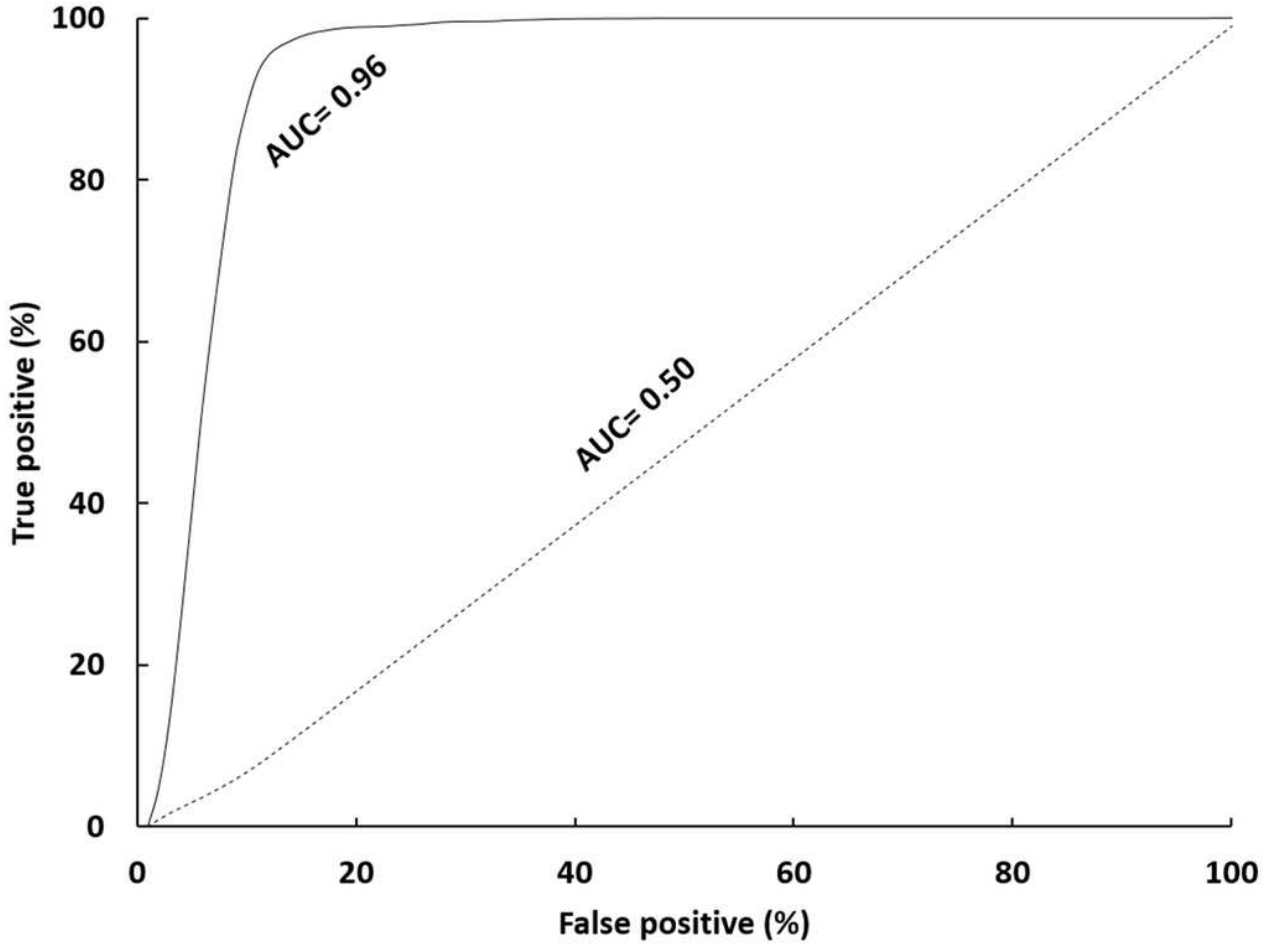


Figure 8

ROC curves assessment of the FAHP model

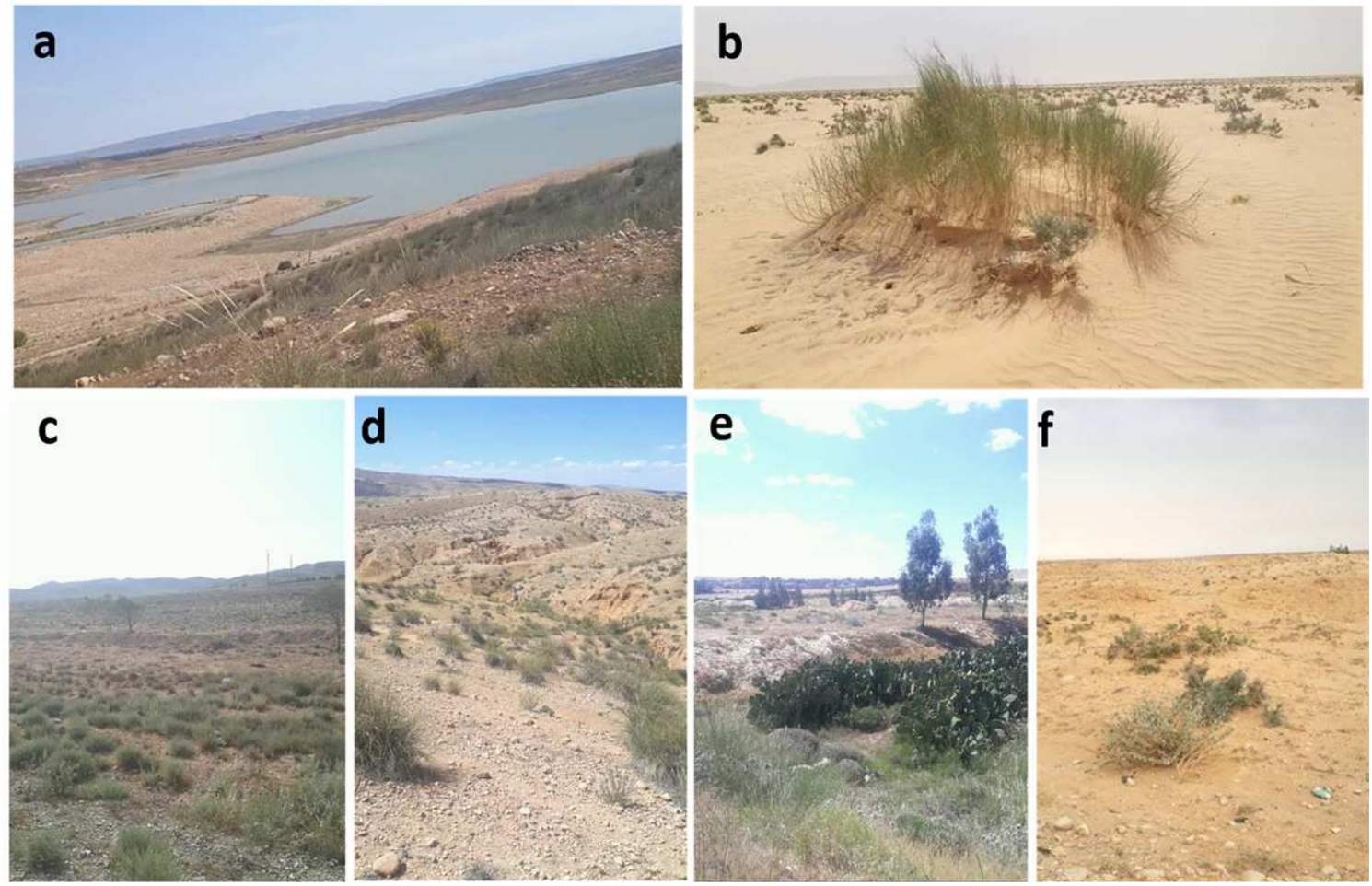


Figure 9

Example of field investigation over the study areas. (a) Safsaf El-Oussera dam (Safsaf El-Oussera), (b) Nebka with mobile sand dunes, dominate by Aristida pungens Desf (Negrine), (c) degraded rangeland dominated by Artemisia herba-alba Asso, Artemisia campestris L (Safsaf El-Oussera), (d) degraded rangeland dominated by Stipa tenacissima L (Bir El Ater), (e) prickly pear (Opuntia ficus-indica L) plantations (Bir El Ater), (f) Nebka with fixed sand dunes, dominate by Aristida pungens Desf (Negrine)